Acoustic behavior of a rigidly backed poroelastic layer with periodic resonant inclusions by a multiple scattering approach

Thomas Weisser,[1,a)] Jean-Philippe Groby,[1] Olivier Dazel,[1] François Gaultier,[1] Elke Deckers,[2] Sideto Futatsugi,[3] and Luciana Monteiro[3]
[1]*Laboratoire d'Acoustique de l'Université du Maine, UMR6613 CNRS/Université du Maine, 72085 Le Mans Cedex 9, France*
[2]*Department of Mechanical Engineering, Katholieke Universiteit Leuven, 3001 Heverlee, Belgium*
[3]*Embraer, São José dos Campos, 12227-901, Brazil*

(Received 7 July 2015; revised 16 November 2015; accepted 12 January 2016; published online 3 February 2016)

The acoustic response of a rigidly backed poroelastic layer with a periodic set of elastic cylindrical inclusions embedded is studied. A semi-analytical approach is presented, based on Biot's 1956 theory to account for the deformation of the skeleton, coupling mode matching technique, Bloch wave representation, and multiple scattering theory. This model is validated by comparing the derived absorption coefficients to finite element simulations. Numerical results are further exposed to investigate the influence of the properties of the inclusions (type, material properties, size) of this structure, while a modal analysis is performed to characterize the dynamic behaviors leading to high acoustic absorption. Particularly, in the case of thin viscoelastic membranes, an absorption coefficient larger than 0.8 is observed on a wide frequency band. This property is found to be due to the coupling between the first volume mode of the inclusion and the trapped mode induced by the periodic array and the rigid backing, for a wavelength in the air smaller than 11 times the material thickness. © *2016 Acoustical Society of America*. [http://dx.doi.org/10.1121/1.4940669]

[OU] Pages: 617–629

I. INTRODUCTION

This work was initially motivated by the study of acoustic metamaterials for acoustic absorption, especially in the aeronautical industry where both weight and space remain of critical concern. Although porous materials, such as foams, are commonly used, they suffer from a lack of absorption at low frequencies compared to their efficiency at higher ones. This difficulty is usually overcome by multi-layering.[1] However, while reducing the impedance mismatch at the air-material interface, the efficiency of such devices relies on the allowable thickness.

Over the past ten years, macroscopically inhomogeneous foams have proved to be a promising alternative. Seminal works by Boutin and Olny[2] on double-porosity materials showed that absorption properties of a porous layer can be enhanced by the resonance of the foam microstructure, excited by the macro-pores obtained by drilling holes through the thickness of a regular porous plate.[2,3] Initially based on homogenization techniques, such materials have also been modeled using finite element methods,[4,5] possibly combined with a topological optimization algorithm.[6] This double-porosity approach has been further adapted by Gourdon and Seppi[7] to account for porous material inclusions instead of air cavities. In addition, De Ryck *et al.* derived the equations describing acoustic wave propagation in a macroscopically inhomogeneous rigid-frame porous medium,[8] from the alternative formulation of Biot's theory.[9] These theoretical developments can be used to model and to design poroelastic layer with continuous-varying properties (e.g., functionally graded foams[10]).

Following this research and the growing interest in acoustic metamaterials,[11–15] the concept of metaporous material has been later developed to simultaneously take advantage of the damping effects of the host foam material, as well as the scattering effects and resonances of embedded inclusions. The study of multiple scattering in rigid-frame porous materials has been initiated by Tournat *et al.*[16] who considered the transmission through a porous medium in which randomly arranged small-sized metallic rods are embedded transversally. Using a modified formulation of the independent scattering approximation (called ISAβ approach), this homogenized medium was shown to exhibit a decreased acoustic transmission.

This finding, together with the evidence of increased optical absorption in rough surfaces (first studied by Wood,[17] and partially explained by Wirgin and Lopez-Rios[18]), led Groby *et al.*[19] to investigate, using the multipole method, the acoustic properties of a rigid-frame porous plate (i.e., under an equivalent fluid hypothesis) in which is embedded a periodic set of scatterers, whose size cannot be neglected compared to the acoustic wavelength. If the radii of these periodic inclusions are comparable to the acoustic wavelength and the inclusions are considered as rigid, then a perfect absorption coefficient can be observed at frequencies below the natural frequency of the first mode of the porous plate. These phenomena are mainly due to a decrease of the transmission coefficient in the case of one grating of inclusions, or to bandgaps with total absorption peaks in the case of a finite depth sonic crystal (multi-layered grating).[20] Groby *et al.* explained the influence of the periodic inclusions on the absorption coefficient as

[a)]Present address: Université de Haute-Alsace, Laboratoire MIPS, Mulhouse, France. Electronic mail: thomas.weisser@uha.fr

soliciting additional acoustic modes which trap the energy inside the structure and dissipate the acoustic energy through viscous and thermal effects in the material pores. When the porous layer is backed by a flat, rigid surface and when only one inclusion per unit cell is embedded, an additional trapped mode can be excited. This results in a perfect absorption peak at a frequency below the usual quarter-wavelength resonance frequency, in the homogeneous layer case.[19]

More recently, the works of Lagarrigue *et al.*[21] focused on metaporous materials with periodic resonant inclusions, based on a rigid assumption for both the frame of the porous material and solid inclusions. Using a finite element approach, the authors studied the influence of the geometry and the orientation of split-ring resonators on the acoustic absorption, resulting in a combination between their resonances and the previous trapped mode phenomena. They also achieved large-band absorption by designing supercells composed of variously configured resonators. Finally, while these references and the present article are related to two-dimensional configurations, three-dimensional configurations have also been investigated.[22,23]

The purpose of the present article is to extend the concept of metaporous material to the case of poroelastic host foams. Indeed, when the elastic skeleton of a porous material is excited and the considered frequency band lies below the decoupling frequency, wave propagation mechanisms must be modeled using the full Biot's theory.[24] By adapting the multiple scattering approach to account for the associated Biot waves, a semi-analytical model is proposed to predict the acoustic behavior of such acoustic metamaterials. After validating the approach with finite element simulations and comparing it to an equivalent fluid approach, enhanced acoustic properties are illustrated in the case of thin shell inclusions.

II. FORMULATION OF THE PROBLEM

A. Description of the configuration

The problem, depicted in Fig. 1, is assumed to be invariant with respect to the Cartesian direction $\boldsymbol{x}_3$. The studied configuration consists in a rigidly backed poroelastic domain $\Omega^{[1]}$ of thickness H. The periodic array of cylindrical inclusions is composed of an infinite set of elastic domains $\Omega^{[2]}$ with external radii a (internal radii b in the case of shell inclusions) and period d. The surrounding air medium occupies the upper domain denoted $\Omega^{[0]}$. The incident wave vector $\boldsymbol{k}^{\text{inc}}$ lies in the sagittal plane and the associated incidence angle γ^{inc} is defined counterclockwise from the positive $\boldsymbol{x}_1$ axis.

In order to deal with harmonic frequency-dependent quantities, the pressure and the other fields are considered through their Fourier transform, using the following time convention: $\tilde{p}(\boldsymbol{x},t) = \int_{-\infty}^{\infty} p(\boldsymbol{x},\omega)e^{-\mathrm{i}\omega t}\,\mathrm{d}\omega$. To lighten the following theoretical developments, this ω-dependency will be dropped. The incident wave is classically expressed using the associated pressure field, of amplitude A^{inc}, such as $p^{\text{inc}}(\boldsymbol{x}) = A^{\text{inc}}e^{\mathrm{i}k_1^{\text{inc}}x_1}e^{-\mathrm{i}k_2^{\text{inc}}(x_2-H)}$, where $k_1^{\text{inc}} = -k^{\text{inc}}\cos\gamma^{\text{inc}}$ and $k_2^{\text{inc}} = k^{\text{inc}}\sin\gamma^{\text{inc}}$.

Considering the plane wave nature of the incident wave and the periodicity of the configuration, the classical Floquet relation, $p(x_1+nd,x_2) = p(x_1,x_2)e^{\mathrm{i}k_1^{\text{inc}}nd}$, $n\in\mathbb{Z}$, for the pressure fields, is further used to bring the study down to determining the various fields in the unit cell of the layer containing one inclusion.

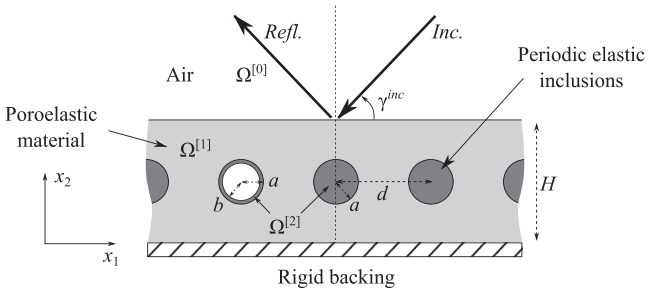

FIG. 1. Cross-sectional plane view of the configuration.

B. Material modeling

Wave propagation mechanisms inside the poroelastic medium $\Omega^{[1]}$ are modeled using the full Biot's theory,[24] which handles both solid and fluid phases of a porous medium (the associated quantities are referred to as $\cdot^s$ and $\cdot^f$, respectively) according to the following constitutive relations:

$$\sigma_{ij}^{s\,[1]} = [(P-2N)\nabla\cdot\boldsymbol{u}^{[1]} + Q\nabla\cdot\boldsymbol{U}^{[1]}]\delta_{ij} + 2Ne_{ij}^{s\,[1]}, \tag{1}$$

$$\sigma_{ij}^{f\,[1]} = (Q\nabla\cdot\boldsymbol{u}^{[1]} + R\nabla\cdot\boldsymbol{U}^{[1]})\delta_{ij}, \tag{2}$$

where σ_{ij}^s and σ_{ij}^f are the components of the stress tensors of both solid and fluid phases, respectively; $\boldsymbol{u}^{[1]}$ and $\boldsymbol{U}^{[1]}$ represent the displacement fields in the solid and the fluid phases, respectively; P, Q, and R are the so-called Biot coefficients, whose expressions can be found in Ref. 24; $e_{ij}^{s\,[1]} = (1/2)(\nabla\boldsymbol{u}^{[1]} + \nabla^T\boldsymbol{u}^{[1]})$ is the linear strain tensor of the solid phase; δ_{ij} denotes the Kronecker delta. These displacements can be further expressed by separately considering the potentials associated with compressional and shear waves, as

$$\boldsymbol{u}^{[1]} = \nabla\varphi_P^{[1]} + \nabla\varphi_A^{[1]} + \nabla\wedge\boldsymbol{\Psi}_S^{[1]}, \tag{3}$$

$$\boldsymbol{U}^{[1]} = \mu_P^{[1]}\nabla\varphi_P^{[1]} + \mu_A^{[1]}\nabla\varphi_A^{[1]} + \mu_S^{[1]}\nabla\wedge\boldsymbol{\Psi}_S^{[1]}, \tag{4}$$

where $\varphi_P^{[1]}$ and $\varphi_A^{[1]}$ are the potentials associated with the so-called "fast" and "slow" compressional waves, respectively, $\boldsymbol{\Psi}_S = \psi_S\boldsymbol{x}_3$ is the potential associated with shear wave and $\mu_P^{[1]}$, $\mu_A^{[1]}$, and $\mu_S^{[1]}$ are coefficients denoting the ratios between the displacements in both phases for each propagation mode.

Moreover, in the case of sound absorbing materials, e.g., foams, material parameters cannot be considered as frequency independent. To model these dissipation phenomena, the five-parameter Johnson–Champoux–Allard (JCA) model is used.[25] The associated frequency-dependent effective density ρ and bulk modulus K are given by

$$\rho(\omega) = \frac{\rho_0}{\phi}\left[\alpha_\infty - \frac{\nu\phi}{\mathrm{i}\omega q_0}F(\omega)\right], \tag{5}$$

$$K(\omega) = \frac{\gamma P_0}{\phi}\left[\gamma - \frac{\gamma-1}{1-\dfrac{\nu'\phi}{\mathrm{i}\omega q_0'}G(\omega)}\right]^{-1}, \tag{6}$$

where ρ_0 is the air density; P_0 the ambient mean pressure; $\nu = \eta/\rho_0 = \mathrm{Pr}\,\nu'$ with η the viscosity of the fluid phase and Pr the Prandtl number; γ is the specific heat ratio; $q_0 = \eta/\sigma$ and $q'_0 = \phi\Lambda'^2/8$ are the static viscous and thermal permeabilities, respectively. The five JCA parameters are the open porosity ϕ, the static airflow resistivity σ (depending on q_0), the tortuosity α_∞ and the viscous and thermal characteristic lengths Λ and Λ', respectively. The frequency-dependent functions $F(\omega)$ and $G(\omega)$ are given by

$$F(\omega) = \left[1 - \left(\frac{2\alpha_\infty q_0}{\phi\Lambda}\right)^2 \frac{\mathrm{i}\omega}{\nu}\right]^{1/2}, \tag{7}$$

$$G(\omega) = \left[1 - \left(\frac{\Lambda'}{4}\right)^2 \frac{\mathrm{i}\omega}{\nu'}\right]^{1/2}. \tag{8}$$

Introducing these complex frequency-dependent coefficients into the wave equations derived from Biot's 1956 theory leads to the so-called Biot–Johnson–Allard model.[26]

The constitutive relation associated with each of the elastic inclusions is classically given by

$$\sigma_{ij}^{[2]} = \lambda^{[2]}\nabla\cdot\boldsymbol{u}^{[2]} + 2\mu^{[2]}e_{ij}^{[2]}, \tag{9}$$

where $\lambda^{[2]}$ and $\mu^{[2]}$ are the Lamé coefficients and $e_{ij}^{[2]}$ corresponds to the linear strain tensor associated with the displacement field inside each inclusion $\boldsymbol{u}^{[2]}$. The latter can also be expressed using potentials $\varphi_P^{[2]}$ and $\boldsymbol{\Psi}_S^{[2]}$ associated with compressional and shear waves, respectively, as

$$\boldsymbol{u}^{[2]} = \nabla\varphi_P^{[2]} + \nabla\wedge\boldsymbol{\Psi}_S^{[2]}. \tag{10}$$

C. Field representations in $\Omega^{[0]}$, $\Omega^{[1]}$, and $\Omega^{[2]}$ and solutions of intermediate problems

The uniqueness of the solution to the forward scattering problem of the incident plane wave, of amplitude A^{inc}, on the metaporous layer is ensured by the radiation condition $p^{[0]}(\boldsymbol{x}) - p^{\mathrm{inc}}(\boldsymbol{x}) \sim$ outgoing waves, for $x_2 \gg H$. The expression of the external pressure field in $\Omega^{[0]}$ can then be derived using the separation of variables and the Floquet relation, as

$$p^{[0]} = \sum_{q\in\mathbb{Z}} e^{\mathrm{i}k_{1q}x_1}\left(A^{\mathrm{inc}}e^{-\mathrm{i}k_{2q}^{[0]}(x_2-H)}\delta_{q0} + R_q e^{\mathrm{i}k_{2q}^{[0]}(x_2-H)}\right), \tag{11}$$

where R_q are the reflection coefficients associated with the qth Bloch mode, $k_{1q} = k_1^{\mathrm{inc}} + 2q\pi/d$, and $k_{2q}^{[0]} = \sqrt{(k^{[0]})^2 - (k_{1q})^2}$, with $\mathrm{Re}(k_{2q}^{[0]}) \geq 0$ and $\mathrm{Im}(k_{2q}^{[0]}) \geq 0$.

At this step of the modeling process, it is more convenient to use Cartesian coordinates to write the field representation inside the poroelastic layer. According to the principle of superposition, this can be seen as the sum of the field diffracted in the plate and the fields diffracted by the inclusions. The potentials associated with the three Biot waves in $\Omega^{[1]}$ (with Ξ representing φ or ψ and X representing P or A when Ξ is φ, and S when Ξ is ψ) can thus be written as

$$\Xi_X^{[1]} = \sum_{q\in\mathbb{Z}} e^{\mathrm{i}k_{1q}x_1}\left(f_q^{[1]X}e^{-\mathrm{i}k_{2q}^{[1]X}x_2} + g_q^{[1]X}e^{\mathrm{i}k_{2q}^{[1]X}x_2}\right) + \sum_{q\in\mathbb{Z}}\sum_{n\in\mathbb{Z}} K_{qn}^{X\pm}C_n^X e^{\mathrm{i}k_{1q}(x_1-x_1^{(0)})\pm\mathrm{i}k_{2q}^{[1]X}(x_2-x_2^{(0)})}, \tag{12}$$

where $f_q^{[1]X}$ and $g_q^{[1]X}$ are amplitude coefficients representing the waves diffracted at the layer boundaries and propagating along the negative and positive $\boldsymbol{x}_2$ direction, respectively; $k_{2q}^{[1]} = \sqrt{(k^{[1]X})^2 - (k_{1q})^2}$, with $\mathrm{Re}(k_{2q}^{[1]X}) \geq 0$ and $\mathrm{Im}(k_{2q}^{[1]X}) \geq 0$, where $k^{[1]}X$ represents the wavenumber associated with the X-type Biot wave; $x_1^{(0)}$ and $x_2^{(0)}$ are the coordinates of the center of the inclusion; and $K_{qn}^{X\pm} = 2(-\mathrm{i})^n e^{\pm\mathrm{i}n\xi_q^X}/(k_{2q}^{[1]X}d)$, with ξ_q such that $k^{[1]X}e^{\mathrm{i}\xi_q^X} = k_{1q} + \mathrm{i}k_{2q}^{[1]X}$, represent the polar to Cartesian coordinates operator; the signs + and − correspond to $x_2 > a$ and $x_2 < a$, respectively. Here, C_n^X are the diffusion coefficients associated with the inclusion of the reference cell, derived from the global multiple scattering problem of the periodic array.

Evaluating the continuity conditions at the upper and lower boundaries of the layer, namely,

$$\begin{aligned} &\sigma_{12}^{s\,[1]} = 0; \quad \sigma_{22}^{s\,[1]} + \sigma_{22}^{f\,[1]} = -p^{[0]}; \\ &\sigma_{22}^{f\,[1]} = -\phi p^{[0]}; \quad \phi U_2^{[1]} + (1-\phi)u_2^{[1]} = U_2^{[0]}; \end{aligned} \tag{13}$$

at $x_2 = H$ and

$$u_1^{[1]} = 0; \quad u_2^{[1]} = 0; \quad U_2^{[1]} = 0; \tag{14}$$

at $x_2 = 0$, leads to the following linear system,

$$\mathcal{M}^q\boldsymbol{f}^q = \boldsymbol{h}^{\mathrm{inc}}A^{\mathrm{inc}}\delta_{q0} + \sum_{n\in\mathbb{Z}}\boldsymbol{h}_{qn}^P C_n^P + \sum_{n\in\mathbb{Z}}\boldsymbol{h}_{qn}^A C_n^A + \sum_{n\in\mathbb{Z}}\boldsymbol{h}_{qn}^S C_n^S, \tag{15}$$

where $\boldsymbol{f}^q \in \mathbb{C}^{7,1}$ is the vector of the unknown amplitude coefficients defined as

$$\boldsymbol{f}^q = [f_q^{[1]P}\ g_q^{[1]P}\ f_q^{[1]A}\ g_q^{[1]A}\ f_q^{[1]S}\ g_q^{[1]S}\ R_q], \tag{16}$$

and $\mathcal{M}^q \in \mathbb{C}^{7,7}$ at each considered frequency. The right-hand side terms of the equation represent source terms associated with the incident wave and the waves of each Biot wave type scattered by the inclusions, expressed in the global Cartesian coordinate system. Detailed expressions of these terms are given in Appendix A.

Locally, the wave scattering problem of a single inclusion, denoted $\Omega^{[2]}$, inside an infinite poroelastic medium, denoted $\Omega^{[1]}$ can be introduced by assuming a pure compressional X-type incident wave, defined by a wave vector $\boldsymbol{k}^{[1]X}$ and an incidence angle γ_P. Considering a polar coordinate system $[\boldsymbol{x} = (r,\theta)]$, centered on the inclusion, the associated displacement potential is given by

$$\varphi^{\mathrm{inc}} = \sum_{n\in\mathbb{Z}} A_n^X J_n(k^{[1]X}r)e^{\mathrm{i}n\theta}, \tag{17}$$

where A_n^X represents the amplitude of the nth mode associated with the decomposition of the incident wave and J_n denotes Bessel functions of the first kind and nth order. The scattered fields can also be described using a modal decomposition of the displacement potentials in the following form:

$$\Xi_Y^{\text{scat}} = \sum_{n\in\mathbb{Z}} A_n^Y T_n^{XY} H_n^{(1)}(k^{[1]X} r) e^{in\theta}, \tag{18}$$

where $Y = P$, A, S, and $H_n^{(1)}$ denote Hankel functions of the first kind and nth order. The T_n^{XY} coefficients, first introduced by Varadan,[27] represent the transition operators associated with the mode conversion phenomena of an incident X-type wave into a scattered Y-type wave, at the interface between the inclusion and the surrounding medium. Similarly, the field propagating inside a full inclusion can be described by the following potentials:

$$\Xi_Y^{[2]} = \sum_{n\in\mathbb{Z}} A_n^X E_n^{XY} J_n(k^{[2]X} r) e^{in\theta}, \tag{19}$$

where the E_n^{XY} coefficients represent the mode conversion inside the elastic inclusion. All these transition coefficients are determined by applying the boundary conditions at the interface between the inclusion and the surrounding medium using the previous expressions of the various potentials. This finally leads to solving the following linear matrix system:

$$\mathcal{D}_n \boldsymbol{t}_n^X = \boldsymbol{s}_n^X, \tag{20}$$

where $\mathcal{D}_n$ is the global scattering matrix, $\boldsymbol{t}_n^X$ is the vector of the unknown transition coefficients,

$$\boldsymbol{t}_n^X = [T_n^{XP} \quad T_n^{XA} \quad T_n^{XS} \quad E_n^{XP} \quad E_n^{XS}]^T, \tag{21}$$

associated with an incident X-type wave, described by the source vector $\boldsymbol{s}_n^X$. Expressions of the boundary conditions, $\mathcal{D}_n$ matrices and $\boldsymbol{s}_n^X$ vectors derived for both full elastic and shell inclusions (which are discussed later in Sec. III B) are given in Appendix B. It can also be noted that the size of these matrix systems depends on the number of modes retained for the initial modal decomposition. The numerical criterion to determine the truncation order of the decomposition is given in Appendix D.

D. Multiple scattering approach

Several studies have investigated the scattering of plane waves by a single or a pair of inclusions in different configurations: elastic waves and a viscolelastic inclusion,[28] poroelastic inclusions in an acoustic medium,[29] compressional waves and an elastic inclusion in a poroelastic medium.[30] However, in this study, the inclusions composing the periodic set cannot be considered as isolated.

The multiple scattering theory initially developed by Záviška,[31] and further promoted by Twersky,[32] is characterized by the fact that the field diffracted by a single inclusion only depends on its geometric or acoustic properties: the multiple scattering model then describes the interactions between all the inclusions. Hence, the incident field on a given inclusion is composed of the initial incident field and also of the field scattered by the other inclusions. While lots of studies concern multiple wave scattering in elastic media[33] only a few have focused on porous media, either restricting to homogenization approaches dedicated to random inclusion sets,[34] or equivalent fluid approaches.[35,36] Therefore, the following theoretical developments constitute an original attempt to handle the full Biot's theory, allowing to accurately describe poroelastic media with embedded periodic inclusions, through the multiple scattering formalism.

According to the previous definition and considering the reference inclusion of the periodic set, an expression of the displacement potentials can be directly derived by extending the single scattering problem, namely,

$$\Xi_X^{[1]} = \sum_{n=-\infty}^{+\infty} C_n^X H_n^{(1)}(k^{[1]X} r) e^{in\theta} + \sum_{n=-\infty}^{+\infty} \mathcal{A}_n^X J_n(k^{[1]X} r) e^{in\theta}, \tag{22}$$

where $\mathcal{A}_n^X$ are the amplitude coefficients associated with the global source terms generated by the scattering of an incoming X-type Biot wave. These terms can be identified by transposing Eq. (12) from its global Cartesian form to the local cylindrical coordinate system. However, as emphasized by Eq. (15), the amplitude coefficients $f_q^{[1]X}$ and $g_q^{[1]X}$ also depend on the scattering coefficients C_n^X. Hence, considering the complexity of this linear system, a semi-analytical solution is further handled in the form

$$\boldsymbol{f}^q = \mathcal{F}_q^{\text{inc}} \delta_q + \sum_{n=-\infty}^{+\infty} \mathcal{F}_{qn}^P C_n^P + \sum_{n=-\infty}^{+\infty} \mathcal{F}_{qn}^A C_n^A + \sum_{n=-\infty}^{+\infty} \mathcal{F}_{qn}^S C_n^S, \tag{23}$$

by numerically evaluating $\mathcal{F}_q^{\text{inc}} = [\mathcal{M}^q]^{-1} \boldsymbol{h}^{\text{inc}}$ and $\mathcal{F}_{qn}^X = [\mathcal{M}^q]^{-1} \boldsymbol{h}_{qn}^X$, using the system given Eq. (15). As an example, substituting these expressions into Eq. (12) and focusing on $\varphi_P^{[1]}$, whose amplitude coefficients are located in lines 1 and 2 inside $\boldsymbol{f}_q$ [denoted "$^{(1)}$." and "$^{(2)}$.," respectively] gives

$$\begin{aligned}
\varphi_P^{[1]} = {} & \sum_{n=-\infty}^{+\infty} C_n^P H_n^{(1)}(k^{[1]P} r) e^{in\theta} + \sum_{n=-\infty}^{+\infty} \sum_{m=-\infty}^{+\infty} \sigma_{mn}^P C_m^P J_n(k^{[1]P} r) e^{in\theta} + \sum_{n=-\infty}^{+\infty} \sum_{q=-\infty}^{+\infty} ({}^{(1)}\mathcal{F}_q^{\text{inc}} \delta_q L_{nq}^{P-} e^{-ik_{2q}^{[1]P} x_2^{(0)}} + {}^{(2)}\mathcal{F}_q^{inc} \delta_q L_{nq}^{P+} e^{ik_{2q}^{[1]P} x_2^{(0)}}) \\
& \times e^{ik_{1q} x_1^{(0)}} J_n(k^{[1]P} r) e^{in\theta} + \sum_{n=-\infty}^{+\infty} \sum_{q=-\infty}^{+\infty} \sum_{m=-\infty}^{+\infty} [({}^{(1)}\mathcal{F}_{qm}^P C_m^P + {}^{(1)}\mathcal{F}_{qm}^A C_m^A + {}^{(1)}\mathcal{F}_{qm}^S C_m^S) L_{nq}^{P-} e^{-ik_{2q}^{[1]P} x_2^{(0)}} \\
& + ({}^{(2)}\mathcal{F}_{qm}^P C_m^P + {}^{(2)}\mathcal{F}_{qm}^A C_m^A + {}^{(2)}\mathcal{F}_{qm}^S C_m^S) L_{nq}^{P+} e^{ik_{2q}^{[1]P} x_2^{(0)}}] e^{ik_{1q} x_1^{(0)}} J_n(k^{[1]P} r) e^{in\theta},
\end{aligned} \tag{24}$$

where σ^P_{mn} is similar to the so-called Schlömilch series (or lattice sum), defined by

$$\sigma^X_{mn} = \sum_{p=1}^{+\infty} H^{(1)}_{m-n}(k^{[1]X}pd)\left[(-1)^{m-n}e^{\mathrm{i}k_1^{[1]X}pd} + e^{-\mathrm{i}k_1^{[1]X}pd}\right], \tag{25}$$

accounting for the field scattered by all the inclusions except the reference inclusion; and $L^{X\pm}_{nq} = \mathrm{i}^n e^{\mp \mathrm{i}n\xi^X_q}$. Comparing this expression to Eq. (22) leads to

$$\mathcal{A}^X_n = \sum_{m=-\infty}^{+\infty}\left(\sigma^X_{mn}C^X_m + \sum_{q=-\infty}^{+\infty} Q^{PX}_{mnq}C^P_m + \sum_{q=-\infty}^{+\infty} Q^{AX}_{mnq}C^A_m + \sum_{q=-\infty}^{+\infty} Q^{SX}_{mnq}C^S_m\right) + \sum_{q=-\infty}^{+\infty} S^X_{nq}, \tag{26}$$

where Q^{YX}_{mnq} and S^X_{nq} are coefficients whose expressions are given in Appendix C.

Finally, assuming that the scattering coefficient associated with an X-type Biot wave is composed of the conversion of the various incoming amplitudes through the previously defined transition operators, Eq. (18), as

$$C^X_n = T^{PX}_n\mathcal{A}^P_n + T^{AX}_n\mathcal{A}^A_n + T^{SX}_n\mathcal{A}^S_n, \tag{27}$$

and introducing the developed expressions of the source terms given in Eq. (26), the following linear matrix system can be derived:

$$\begin{bmatrix}
\boldsymbol{I}_d - [\boldsymbol{T}^{PP}(\bar{\boldsymbol{\sigma}}^P + \boldsymbol{Q}^{PP}) + \boldsymbol{T}^{AP}\boldsymbol{Q}^{PA} + \boldsymbol{T}^{SP}\boldsymbol{Q}^{PS}] & -[\boldsymbol{T}^{PP}\boldsymbol{Q}^{AP} + \boldsymbol{T}^{AP}(\bar{\boldsymbol{\sigma}}^A + \boldsymbol{Q}^{AA}) + \boldsymbol{T}^{SP}\boldsymbol{Q}^{AS}] & \dots \\
-[\boldsymbol{T}^{PA}(\bar{\boldsymbol{\sigma}}^P + \boldsymbol{Q}^{PP}) + \boldsymbol{T}^{AA}\boldsymbol{Q}^{PA} + \boldsymbol{T}^{SA}\boldsymbol{Q}^{PS}] & \boldsymbol{I}_d - [\boldsymbol{T}^{PA}\boldsymbol{Q}^{AP} + \boldsymbol{T}^{AA}(\bar{\boldsymbol{\sigma}}^A + \boldsymbol{Q}^{AA}) + \boldsymbol{T}^{SA}\boldsymbol{Q}^{AS}] & \dots \\
-[\boldsymbol{T}^{PS}(\bar{\boldsymbol{\sigma}}^P + \boldsymbol{Q}^{PP}) + \boldsymbol{T}^{AS}\boldsymbol{Q}^{PA} + \boldsymbol{T}^{SS}\boldsymbol{Q}^{PS}] & -[\boldsymbol{T}^{PS}\boldsymbol{Q}^{AP} + \boldsymbol{T}^{AS}(\bar{\boldsymbol{\sigma}}^A + \boldsymbol{Q}^{AA}) + \boldsymbol{T}^{SS}\boldsymbol{Q}^{AS}] & \dots
\end{bmatrix}$$

$$\begin{bmatrix}
-[\boldsymbol{T}^{PP}\boldsymbol{Q}^{SP} + \boldsymbol{T}^{AP}\boldsymbol{Q}^{SA} + \boldsymbol{T}^{SP}(\bar{\boldsymbol{\sigma}}^S + \boldsymbol{Q}^{SS})] \\
-[\boldsymbol{T}^{PA}\boldsymbol{Q}^{SP} + \boldsymbol{T}^{AA}\boldsymbol{Q}^{SA} + \boldsymbol{T}^{SA}(\bar{\boldsymbol{\sigma}}^S + \boldsymbol{Q}^{SS})] \\
\boldsymbol{I}_d - [\boldsymbol{T}^{PS}\boldsymbol{Q}^{SP} + \boldsymbol{T}^{AS}\boldsymbol{Q}^{SA} + \boldsymbol{T}^{SS}(\bar{\boldsymbol{\sigma}}^S + \boldsymbol{Q}^{SS})]
\end{bmatrix}
\begin{bmatrix} \boldsymbol{C}^P \\ \boldsymbol{C}^A \\ \boldsymbol{C}^S \end{bmatrix}
= \begin{bmatrix}
\boldsymbol{T}^{PP}\boldsymbol{S}^P + \boldsymbol{T}^{AP}\boldsymbol{S}^A + \boldsymbol{T}^{SP}\boldsymbol{S}^S \\
\boldsymbol{T}^{PA}\boldsymbol{S}^P + \boldsymbol{T}^{AA}\boldsymbol{S}^A + \boldsymbol{T}^{SA}\boldsymbol{S}^S \\
\boldsymbol{T}^{PS}\boldsymbol{S}^P + \boldsymbol{T}^{AS}\boldsymbol{S}^A + \boldsymbol{T}^{SS}\boldsymbol{S}^S
\end{bmatrix}, \tag{28}$$

where $\boldsymbol{T}^{XY}$, $\bar{\boldsymbol{\sigma}}^X$, $\boldsymbol{Q}^{XY}$, and $\boldsymbol{S}^X$ are matrices of elements $T^{XY}_n\delta_{ij}$, σ^X_{ji}, $\sum_{q\in\mathbb{Z}}Q^{XY}_{mnq}$, and $\sum_{q\in\mathbb{Z}}S^X_{nq}$, respectively; $\boldsymbol{I}_d$ denotes the identity matrix.

Once this system has been numerically solved using the truncation formulas given in Appendix D, the obtained scattering coefficients are substituted into Eq. (23) to determine the components of vector $\boldsymbol{f}_q$, which includes the reflexion coefficients.

III. NUMERICAL RESULTS AND DISCUSSION

The following numerical calculations are related to the previously described configuration (Fig. 1) with $H = d = 2$ cm, using the material properties given in Table I. This porous material has been provided by the industrial partner Embraer (São José dos Campos, Brazil) and is typically used, with a larger thickness, for aircraft cabin insulation.

A. Elastic inclusions

At first, the influence of a periodic set of elastic full inclusions is investigated. Previous studies[19,20,36] performed under a motionless skeleton hypothesis have shown that embedding inclusions is particularly efficient to enhance the absorption properties of small thickness foam slabs, especially below the so-called quarter-wavelength frequency of the slow wave. In this section, calculations were run considering both steel inclusions ($\rho_e = 7800\,\mathrm{kgm^{-3}}$, $c_p = 5100\,\mathrm{ms^{-1}}$, and $c_s = 1480\mathrm{ms^{-1}}$)

TABLE I. Parameters of the poroelastic material.

Description	Symbol	Value
Porosity	ϕ	0.989
Resistivity	σ	8060 $\mathrm{Nsm^{-4}}$
Tortuosity	α_∞	1.0
Viscous characteristic length	Λ	214 μm
Thermal characteristic length	Λ'	214 μm
Density	ρ	6.1 $\mathrm{kgm^{-3}}$
Young's modulus	E	56 544 $\mathrm{kgm^{-1}s^{-2}}$
Poisson's ratio	ν	0.21
Structural loss factor	η	0.02

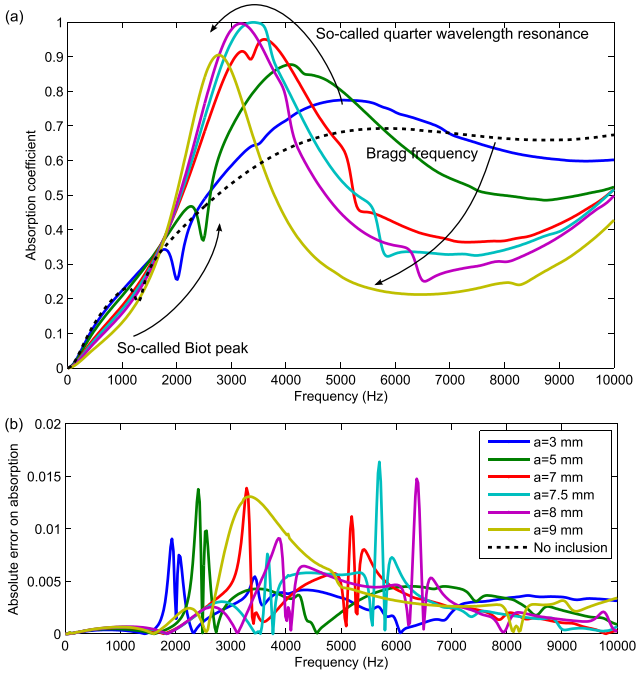

FIG. 2. (Color online) (a) Absorption coefficients at normal incidence for a 2-cm periodic set of steel inclusions embedded in a 2-cm thick poroelastic plate for various radii; (b) associated errors comparing to finite-element approach.

and Plexiglas inclusions ($\rho_e = 1180\,\mathrm{kg\,m^{-3}}$, $c_p = 2700\,\mathrm{m\,s^{-1}}$, and $c_s = 1370\mathrm{ms^{-1}}$), yet leading to quite similar results. The exposed results will therefore focus on steel inclusions.

To assess the results derived from the semi-analytical model, an in-house finite element code has been developed and used. Based on quadratic triangular elements, this code handles both excitation by a plane wave and periodicity conditions. Figure 2(a) shows the values of the absorption coefficients using the proposed approach, which are further compared to the finite element values, as illustrated by the associated absolute error curves, Fig. 2(b). A mesh size of six elements per wavelength is applied. A global error lower than 0.02 is observed, illustrating a very good agreement over the whole frequency band and for the various radii. It can also be noticed that the peaks are related to resonance frequencies, which are classically overestimated by finite element approaches. While such errors can be typically reduced using mesh refinement, a convergence analysis is beyond the scope of this article. Hence, both approaches can be considered as cross validated.

Figure 2(a) gives the absorption coefficients calculated with the proposed method for a 2-cm thick foam plate with a 2-cm periodic set of steel inclusion of radius $a \in [3\,\mathrm{mm};9\,\mathrm{mm}]$. It can be noticed that the behavior of the structure is similar to the equivalent fluid behavior, depicted in Fig. 3 (dashed lines), and that the optimal configuration leading to a perfect absorption can be directly translated from one case to the other. This clearly indicates that the inclusions can be considered as rigid. When increasing the radius of the inclusions, the frequency of the

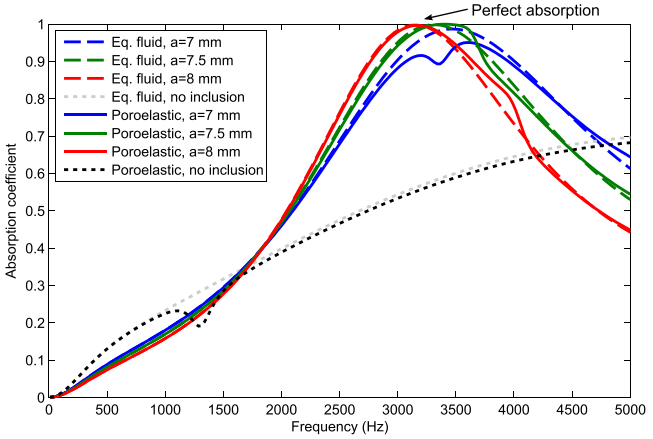

FIG. 3. (Color online) Comparison of the previous absorption coefficients with those calculated under an equivalent fluid hypothesis for various radii.

first absorption peak shifts down, its amplitude increases up to one and then decreases, resulting in a perfect absorption at a frequency lower than the quarter-frequency limit. A trapped mode is then excited, trapping the energy between the inclusions and the rigid backing. Hence, the whole structure can be seen as a resonating absorber:[37] modifying the radius of the inclusion changes the leakage of this resonator, which is then exactly compensated by the losses in the poroelastic material. A critical coupling condition[38,39] is achieved, which generates a perfect absorption at the associated frequency.

The poroelastic aspect of the layer is mainly illustrated by the so-called Biot peak, Fig. 2(a). When the radius of the inclusion increases, its frequency shifts toward higher frequencies, depicting a stiffening of the structure (already observed by Zieliński[40]). Moreover, as observed Fig. 3 for $a = 7.5\,\mathrm{mm}$ or 8 mm (solid lines), when this frequency gets slightly higher than the trapped mode frequency, the absorption increases due to a solid–fluid coupling.

Another interesting comment can be made by decomposing the absorption following the different dissipation

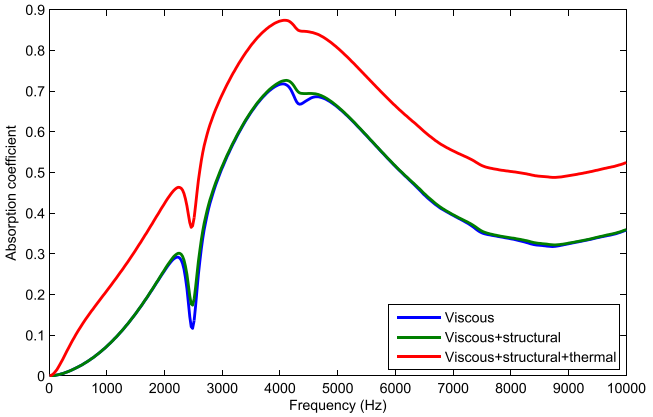

FIG. 4. (Color online) Decomposition of the absorption phenomena for a 2-cm periodic set of steel inclusions of radius $a = 5\,\mathrm{mm}$ embedded in a 2-cm thick poroelastic plate, using FEM approach.

mechanisms inside the metaporous material. This can be easily performed using the in-house finite element approach and the expressions proposed in Ref. 41. As an example, Fig. 4 shows the results derived in the case of inclusions of radii 5 mm (similar comments can be made for other values of the radii). The different parts of the absorption are represented in a cumulative way. It can be noticed that the main part is associated with viscous and thermal effects. In particular, the decrease of absorption around 2.5 kHz is due to a reduction of the viscous effects as the solid Biot wave (corresponding to small relative displacements of the fluid phase with respect to the solid phase) is excited.

The possible modes of the structure are typically associated either to the resonances of the inclusions (not appearing in this case) or to the resonances of the plate induced by the periodic array, or to the resonances of the system as a whole. According to previous analysis, the excitation of Lamb-like modes was expected due to the inclusions. Figures 5(a) and 5(b) depict the real part of the velocity and the imaginary part of the roots of the determinant of matrix $\mathcal{M}^q$, Eq. (15), respectively, which allows to derive these Lamb-like modes of the poroelastic plate.

It can be observed, see Fig. 6, that while the mode associated with the fluid phase (i.e., modified mode of the backed plate) is excited by the periodic set of inclusions, the Lamb-like modes are not (Fig. 2). Moreover, the velocity of the first Bloch wave intersects the first Lamb-like mode at around 3250 Hz, which does not translate on the absorption curve, Fig. 2. This can be due to the fact that the embedded periodic set makes the structure stiffer and therefore makes the Lamb-like modes more difficult to excite. This is confirmed by Fig. 6 where the A_0 mode is only excited without inclusions at oblique incidence, leading to a large absorption peak. In this last case, the absorption coefficient is similar to the one derived under the assumption of motionless porous layer.

B. Resonant inclusions: Thin shell example

As previously emphasized, the advantage of the poroelastic approach is to handle resonant elastic inclusions without loss of generality, as investigated in this section. Among the various types of elastic resonators, thin elastic shells, i.e., membranes, were chosen. High-contrast steel shells of thickness $h = a - b = 200\,\mu$m were first tested, leading to the same results as in Sec. III A. Therefore, rubber shells with mechanical parameters extracted from the literature[42] were used: $E = 1.9 \times 10^6 - i\omega 796$ Pa, $\nu = 0.48$, $\rho_e = 1800$ kg m^{-3}.

Once again, the proposed absorption curves have been compared to finite element computations, showing very good agreement [these are similar to Fig. 2(b) and have been omitted to lighten the article]. In this case, the mesh is more refined than in the previous case in order to handle the small thickness of the shells, corresponding to the characteristic dimension of the mesh. Although very small errors have been observed on resonance peaks, both models are considered as cross validated. This also emphasized one advantage of the proposed approach which does not suffer from aspect ratio issues.

Figure 7 shows the associated absorption curves for the same 2-cm thick poroelastic layer with a 2-cm periodic set of rubber shell inclusions of radii $a \in [7\,\text{mm}; 9\,\text{mm}]$.

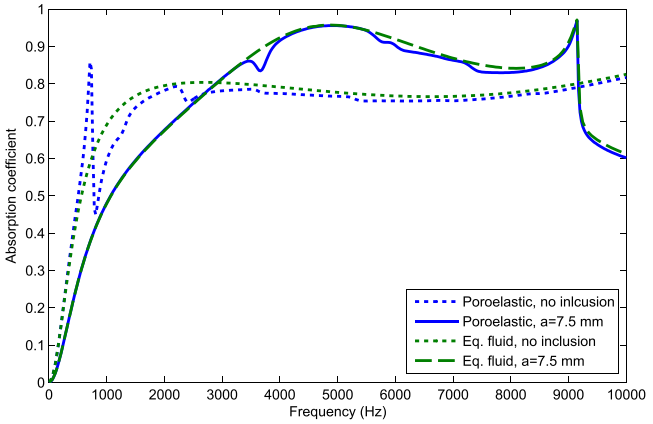

FIG. 6. (Color online) Absorption coefficient at oblique incidence $\gamma^{\text{inc}} = \pi/6$ for both motionless and poroelastic plates.

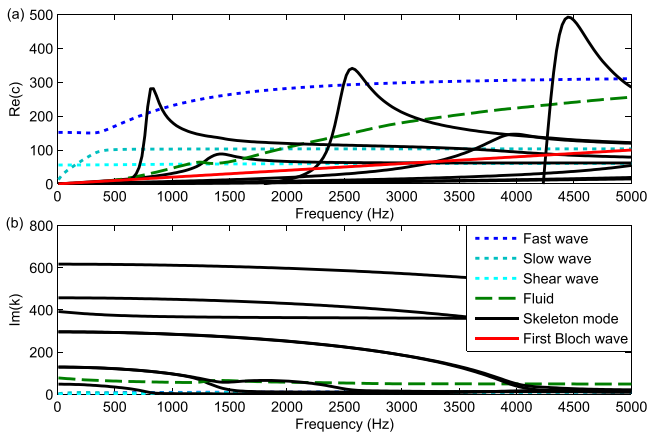

FIG. 5. (Color online) (a) Real part of the velocity of the poroelastic plate modes; (b) imaginary part of the wave number of the poroelastic plate modes.

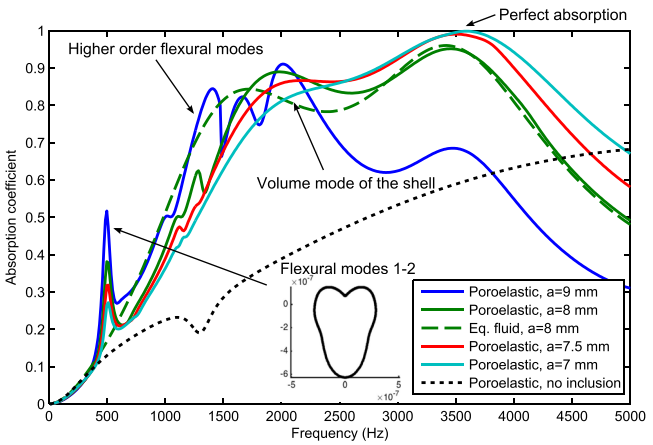

FIG. 7. (Color online) Absorption coefficient at normal incidence for a 2-cm periodic set of thin shell inclusions embedded in a 2-cm thick poroelastic plate of various radii.

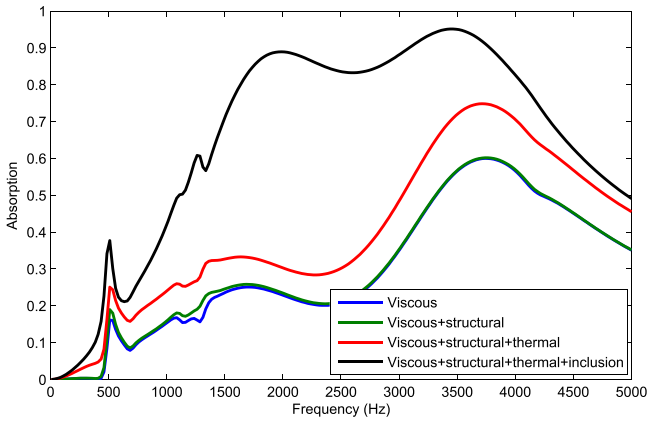

FIG. 8. (Color online) Decomposition of the absorption phenomena for a 2-cm periodic set of thin shell inclusions of radius $a = 8$ mm embedded in a 2-cm thick poroelastic plate, using FEM approach.

First, it can be noted that perfect absorption is obtained at $a = 7$ mm and not at $a = 7.5$ mm as observed for equivalent fluid and elastic inclusions. This confirms that these shell inclusions cannot be considered as rigid and that they interact with the poroelastic plate. It is further illustrated by comparing both solid and dashed green curves ($a = 8$ mm), Fig. 7: the equivalent fluid approach is clearly missing a part of the dynamic behavior due to the structure of the inclusion. Indeed, on the poroelastic curves, two types of resonance of the inclusions are observed: flexural resonances occur around 500 Hz and 1250 Hz (these are not noticeable on the equivalent fluid curve), and the first volume resonance is located around 2500 Hz. This latter is readily affected by the motion of the membrane, as shown in the case of Helmholtz resonators.[43] Furthermore, while the quality factor of the flexural resonances is large, it is very low for the volume resonance, leading to a large absorption at a frequency lower than the perfect absorption frequency. On the contrary, while the equivalent fluid curve clearly exhibits the volume mode of the inclusions, whose frequency is down-shifted by the less stiff boundary conditions between the equivalent fluid medium and the solid inclusions, no flexural mode can be observed.

The contribution of each mode can be further determined by looking at the absolute value of the determinant of matrix $\mathcal{D}_n$ ($n \in \mathbb{Z}$), Eq. (20), or by increasing the number of diffraction coefficients in the calculation. By doing so, the volume resonance is found to be excited through the 0th order diffraction coefficient, i.e., the pressure field inside the shell is uniform. This mode, together with the trapped mode associated with the fluid phase, thus, lead to a large absorption. While the analysis of $\det(\mathcal{D}_n)$ for $n = 0$, $n = \pm 1$, and $n = \pm 2$ exhibits a minimum around 500 Hz, only $n = \pm 1$ and $n = \pm 2$ lead to an absorption peak at these frequencies. At normal incidence, the 0th order flexural mode cannot be excited because of the presence of the neighboring inclusions, which is not the case for higher diffraction orders. As depicted by the inset Fig. 7, representing the angular deformation of the shell for $a = 7.5$ mm, this peak is also due to a combination between these two modes. It can be noted that this frequency corresponds to a wavelength in the air which is 34 times larger than the current thickness of the structure.

Moreover, looking at a wide band behavior, it is particularly interesting to note that the absorption coefficient of the structure for $a \in [7\,\text{mm}; 8\,\text{mm}]$ remains larger than 0.8 between 1500 Hz and 4250 Hz, the lower frequency corresponding to a wavelength in the air that is 11 times larger than the thickness of the structure.

Finally, Fig. 8 shows the decomposition of the total absorption into each dissipation mechanism and once more illustrates the strength of Biot's theory as both the inclusions and the frame are solicited. Most of the energy is dissipated within the inclusion between 1.5 and 3 kHz. This confirms the previous remarks: the first resonance is due to the inclusion and the second resonance is due to the trapped mode of the fluid phase, which involves dissipation by viscous effects.

IV. CONCLUSION

A semi-analytical model of a metaporous material composed of a rigidly backed poroelastic layer with embedded periodic resonant inclusions has been presented. The deformation of the porous material is handled using the full Biot's theory, and the complex behavior of the associated waves inside the structure is modeled using both Bloch wave decomposition and multiple scattering theory. The accuracy of the approach has been cross validated with regard to an in-house finite element code. The model has been further used to investigate the acoustic behavior of such structures.

While the derived results were quite similar to the equivalent fluid (i.e., motionless skeleton) results in the case of full elastic inclusions, except concerning the so-called Biot peak, interesting properties were observed for thin elastic shell inclusions. Particularly, the coupling between both the trapped and the first volume modes lead to a high wide band absorption. These modes are highly affected by the motion of the membrane due to the deformation of the skeleton. Moreover, it has been shown that flexural modes of the membrane lead to absorption peak at very low frequencies. Therefore, some targeted large band absorption could be derived by finely tuning the properties of the thin shell inclusions to control the resonance frequencies of the associated flexural modes.

ACKNOWLEDGMENTS

The authors would like to thank Embraer for financially supporting this work. J.-P.G. and O.D. gratefully acknowledge the support from the ANR (Agence Nationale de la Recherche) and FRAE (Fondation de Recherche pour l'Aéronautique et l'Espace) through ANR-project Metaudible No. ANR-13-BS09-0003. E.D. is a postdoctoral fellow of the Research Foundation—Flanders (FWO).

APPENDIX A: MATRICES OF THE DIFFRACTION PROBLEM AT THE POROUS LAYER BOUNDARIES

Considering the vector of unknown amplitudes $\boldsymbol{f}^q$, defined in Eq. (16), evaluating the boundary conditions given in Eqs. (13) and (14) leads to the following $\mathcal{M}^q \in \mathbb{C}^{7,7}$ matrix,

$$
\begin{aligned}
\mathcal{M}^q(1,1) &= 2k_{1q}k_{2q}^{[1]P}e^{-\mathrm{i}k_{2q}^{[1]P}H},\\
\mathcal{M}^q(1,2) &= -2k_{1q}k_{2q}^{[1]P}e^{\mathrm{i}k_{2q}^{[1]P}H},\\
\mathcal{M}^q(1,3) &= 2k_{1q}k_{2q}^{[1]A}e^{-\mathrm{i}k_{2q}^{[1]A}H},\\
\mathcal{M}^q(1,4) &= -2k_{1q}k_{2q}^{[1]A}e^{\mathrm{i}k_{2q}^{[1]A}H},\\
\mathcal{M}^q(1,5) &= [(k_{1q})^2-(k_{2q}^{[1]S})^2]e^{-\mathrm{i}k_{2q}^{[1]S}H},\\
\mathcal{M}^q(1,6) &= [(k_{1q})^2-(k_{2q}^{[1]S})^2]e^{\mathrm{i}k_{2q}^{[1]S}H},\\
\mathcal{M}^q(1,7) &= 0\,,\\
\mathcal{M}^q(2,1) &= [-(P-2N+Q(1+\mu_P^{[1]})\\
&\quad +\mu_P^{[1]}R)(k^{[1]P})^2-2N(k_{2q}^{[1]P})^2]e^{-\mathrm{i}k_{2q}^{[1]P}H},\\
\mathcal{M}^q(2,2) &= [-(P-2N+Q(1+\mu_P^{[1]})\\
&\quad +\mu_P^{[1]}R)(k^{[1]P})^2-2N(k_{2q}^{[1]P})^2]e^{\mathrm{i}k_{2q}^{[1]P}H},\\
\mathcal{M}^q(2,3) &= [-(P-2N+Q(1+\mu_A^{[1]})\\
&\quad +\mu_A^{[1]}R)(k^{[1]A})^2-2N(k_{2q}^{[1]A})^2]e^{-\mathrm{i}k_{2q}^{[1]A}H},\\
\mathcal{M}^q(2,4) &= [-(P-2N+Q(1+\mu_A^{[1]})\\
&\quad +\mu_A^{[1]}R)(k^{[1]A})^2-2N(k_{2q}^{[1]A})^2]e^{\mathrm{i}k_{2q}^{[1]A}H},\\
\mathcal{M}^q(2,5) &= -2Nk_{1q}k_{2q}^{[1]S}e^{-\mathrm{i}k_{2q}^{[1]S}H},\\
\mathcal{M}^q(2,6) &= 2Nk_{1q}k_{2q}^{[1]S}e^{\mathrm{i}k_{2q}^{[1]S}H},\\
\mathcal{M}^q(2,7) &= 1,
\end{aligned}
\tag{A1}
$$

$$
\begin{aligned}
\mathcal{M}^q(3,1) &= -(Q+\mu_P^{[1]}R)(k^{[1]P})^2e^{-\mathrm{i}k_{2q}^{[1]P}H},\\
\mathcal{M}^q(3,2) &= -(Q+\mu_P^{[1]}R)(k^{[1]P})^2e^{\mathrm{i}k_{2q}^{[1]P}H},\\
\mathcal{M}^q(3,3) &= -(Q+\mu_A^{[1]}R)(k^{[1]A})^2e^{-\mathrm{i}k_{2q}^{[1]A}H},\\
\mathcal{M}^q(3,4) &= -(Q+\mu_A^{[1]}R)(k^{[1]A})^2e^{\mathrm{i}k_{2q}^{[1]A}H},\\
\mathcal{M}^q(3,5) &= 0,\\
\mathcal{M}^q(3,6) &= 0,\\
\mathcal{M}^q(3,7) &= \phi,\\
\mathcal{M}^q(4,1) &= -\mathrm{i}k_{2q}^{[1]P}(1-\phi+\mu_P^{[1]}\phi)e^{-\mathrm{i}k_{2q}^{[1]P}H},\\
\mathcal{M}^q(4,2) &= \mathrm{i}k_{2q}^{[1]P}(1-\phi+\mu_P^{[1]}\phi)e^{\mathrm{i}k_{2q}^{[1]P}H},\\
\mathcal{M}^q(4,3) &= -\mathrm{i}k_{2q}^{[1]A}(1-\phi+\mu_A^{[1]}\phi)e^{-\mathrm{i}k_{2q}^{[1]A}H},\\
\mathcal{M}^q(4,4) &= \mathrm{i}k_{2q}^{[1]A}(1-\phi+\mu_A^{[1]}\phi)e^{\mathrm{i}k_{2q}^{[1]A}H},\\
\mathcal{M}^q(4,5) &= -\mathrm{i}k_{1q}(1-\phi+\mu_S^{[1]}\phi)e^{-\mathrm{i}k_{2q}^{[1]S}H},\\
\mathcal{M}^q(4,6) &= -\mathrm{i}k_{1q}(1-\phi+\mu_S^{[1]}\phi)e^{\mathrm{i}k_{2q}^{[1]S}H},\\
\mathcal{M}^q(4,7) &= -\mathrm{i}k_{2q}^{[0]}/(\rho_{[0]}\omega^2),
\end{aligned}
\tag{A2}
$$

$$
\begin{aligned}
\mathcal{M}^q(5,1) &= \mathrm{i}k_{1q},\\
\mathcal{M}^q(5,2) &= \mathrm{i}k_{1q},\\
\mathcal{M}^q(5,3) &= \mathrm{i}k_{1q},\\
\mathcal{M}^q(5,4) &= \mathrm{i}k_{1q},\\
\mathcal{M}^q(5,5) &= -\mathrm{i}k_{2q}^{[1]S},\\
\mathcal{M}^q(5,6) &= \mathrm{i}k_{2q}^{[1]S},\\
\mathcal{M}^q(5,7) &= 0,\\
\mathcal{M}^q(6,1) &= -\mathrm{i}k_{2q}^{[1]P},\\
\mathcal{M}^q(6,2) &= \mathrm{i}k_{2q}^{[1]P},\\
\mathcal{M}^q(6,3) &= -\mathrm{i}k_{2q}^{[1]A},\\
\mathcal{M}^q(6,4) &= \mathrm{i}k_{2q}^{[1]A},\\
\mathcal{M}^q(6,5) &= -\mathrm{i}k_{1q},\\
\mathcal{M}^q(6,6) &= -\mathrm{i}k_{1q},\\
\mathcal{M}^q(6,7) &= 0,
\end{aligned}
\tag{A3}
$$

$$
\begin{aligned}
\mathcal{M}^q(7,1) &= -\mathrm{i}\mu_P^{[1]}k_{2q}^{[1]P},\\
\mathcal{M}^q(7,2) &= \mathrm{i}\mu_P^{[1]}k_{2q}^{[1]P},\\
\mathcal{M}^q(7,3) &= -\mathrm{i}\mu_A^{[1]}k_{2q}^{[1]A},\\
\mathcal{M}^q(7,4) &= \mathrm{i}\mu_A^{[1]}k_{2q}^{[1]A},\\
\mathcal{M}^q(7,5) &= -\mathrm{i}\mu_S^{[1]}k_{1q},\\
\mathcal{M}^q(7,6) &= -\mathrm{i}\mu_S^{[1]}k_{1q},\\
\mathcal{M}^q(7,7) &= 0.
\end{aligned}
\tag{A4}
$$

The right-hand side of Eq. (15) is composed of the following vectors:

$$
\boldsymbol{h}^{\mathrm{inc}} = [\,0\;\; -A^{\mathrm{inc}}\;\; -A^{\mathrm{inc}}\phi\;\; -\mathrm{i}k_{2q}^{[0]}A^{\mathrm{inc}}/(\rho^{[0]}\omega^2)\;\; 0\;\; 0\;\; 0\,]^T,
\tag{A5}
$$

and

$$
\begin{aligned}
\boldsymbol{h}_{qn}^X(1,1) &= 2k_{1q}k_{2q}^{[1]X}K_{qn}^{X+}e^{-\mathrm{i}k_{1q}x_1^{(0)}}e^{\mathrm{i}k_{2q}^{[1]X}(H-x_2^{(0)})},\\
\boldsymbol{h}_{qn}^X(1,2) &= [(P-2N+Q(1+\mu_X^{[1]})\\
&\quad +\mu_X^{[1]}Q)(k[1]X)^2+2N(k_{2q}^{[1]X})^2]\\
&\quad \times K_{qn}^{X+}e^{-\mathrm{i}k_{1q}x_1^{(0)}}e^{\mathrm{i}k_{2q}^{[1]X}(H-x_2^{(0)})},\\
\boldsymbol{h}_{qn}^X(1,3) &= (Q+\mu_X^{[1]}R)(k[1]X)^2K_{qn}^{X+}e^{-\mathrm{i}k_{1q}x_1^{(0)}}e^{\mathrm{i}k_{2q}^{[1]X}(H-x_2^{(0)})},\\
\boldsymbol{h}_{qn}^X(1,4) &= -\mathrm{i}k_{2q}^{[1]X}(1-\phi+\mu_X^{[1]}\phi)K_{qn}^{X+}e^{-\mathrm{i}k_{1q}x_1^{(0)}}e^{\mathrm{i}k_{2q}^{[1]X}(H-x_2^{(0)})},\\
\boldsymbol{h}_{qn}^X(1,5) &= -\mathrm{i}k_{1q}K_{qn}^{X-}e^{-\mathrm{i}k_{1q}x_1^{(0)}}e^{\mathrm{i}k_{2q}^{[1]X}x_2^{(0)}},\\
\boldsymbol{h}_{qn}^X(1,6) &= \mathrm{i}k_{2q}^{[1]X}K_{qn}^{X-}e^{-\mathrm{i}k_{1q}x_1^{(0)}}e^{\mathrm{i}k_{2q}^{[1]X}x_2^{(0)}},\\
\boldsymbol{h}_{qn}^X(1,7) &= \mathrm{i}\mu_X^{[1]}k_{2q}^{[1]X}K_{qn}^{X-}e^{-\mathrm{i}k_{1q}x_1^{(0)}}e^{\mathrm{i}k_{2q}^{[1]X}x_2^{(0)}},
\end{aligned}
\tag{A6}
$$

for $X = P$, A, and

$$
\begin{aligned}
\boldsymbol{h}^S_{qn}(1,1) &= -[(k_{1q})^2 - (k^{[1]S}_{2q})^2]K^{S+}_{qn} e^{-\mathrm{i}k_{1q}x^{(0)}_1} e^{\mathrm{i}k^{[1]S}_{2q}(H-x^{(0)}_2)},\\
\boldsymbol{h}^S_{qn}(1,2) &= -2Nk_{1q}k^{[1]S}_{2q}K^{S+}_{qn} e^{-\mathrm{i}k_{1q}x^{(0)}_1} e^{\mathrm{i}k^{[1]S}_{2q}(H-x^{(0)}_2)},\\
\boldsymbol{h}^S_{qn}(1,3) &= 0,\\
\boldsymbol{h}^S_{qn}(1,4) &= \mathrm{i}k_{1q}(1-\phi+\mu^{[1]}_S\phi)K^{S+}_{qn} e^{-\mathrm{i}k_{1q}x^{(0)}_1} e^{\mathrm{i}k^{[1]S}_{2q}(H-x^{(0)}_2)},\\
\boldsymbol{h}^S_{qn}(1,5) &= \mathrm{i}k^{[1]S}_{2q}K^{S-}_{qn} e^{-\mathrm{i}k_{1q}x^{(0)}_1} e^{\mathrm{i}k^{[1]S}_{2q}x^{(0)}_2},\\
\boldsymbol{h}^S_{qn}(1,6) &= \mathrm{i}k_{1q}K^{S-}_{qn} e^{-\mathrm{i}k_{1q}x^{(0)}_1} e^{\mathrm{i}k^{[1]S}_{2q}x^{(0)}_2},\\
\boldsymbol{h}^S_{qn}(1,7) &= \mathrm{i}k_{1q}\mu^{[1]}_S K^{S-}_{qn} e^{-\mathrm{i}k_{1q}x^{(0)}_1} e^{\mathrm{i}k^{[1]S}_{2q}x^{(0)}_2}.
\end{aligned}
\tag{A7}
$$

APPENDIX B: MATRICES OF THE SINGLE SCATTERING PROBLEMS

In the case of a full cylindrical elastic inclusion, the boundary conditions at $r=a$ between $\Omega^{[1]}$ and $\Omega^{[2]}$ are

$$
u^{[1]}_r = u^{[2]}_r, \quad u^{[1]}_\theta = u^{[2]}_\theta, \quad U^{[1]}_r = u^{[2]}_r, \quad \sigma^{s[1]}_{rr} + \sigma^{f[1]}_{rr} = \sigma^{[2]}_{rr}, \quad \sigma^{s[1]}_{r\theta} = \sigma^{[2]}_{r\theta}. \tag{B1}
$$

Evaluating these continuity conditions leads to the following scattering matrix $\mathcal{D}_n \in \mathbb{C}^{5,5}$,

$$
\begin{aligned}
\mathcal{D}_n(1,1) &= \alpha^{[1]P}\dot{H}^{(1)}_n(\alpha^{[1]P}),\\
\mathcal{D}_n(1,2) &= \alpha^{[1]A}\dot{H}^{(1)}_n(\alpha^{[1]A}),\\
\mathcal{D}_n(1,3) &= \mathrm{i}nH^{(1)}_n(\alpha^{[1]S}),\\
\mathcal{D}_n(1,4) &= -\alpha^{[2]P}\dot{J}_n(\alpha^{[2]P}),\\
\mathcal{D}_n(1,5) &= -\mathrm{i}nJ_n(\alpha^{[2]S}),\\
\mathcal{D}_n(2,1) &= \mathrm{i}nH^{(1)}_n(\alpha^{[1]P}),\\
\mathcal{D}_n(2,2) &= \mathrm{i}nH^{(1)}_n(\alpha^{[1]A}),\\
\mathcal{D}_n(2,3) &= -\alpha^{[1]S}\dot{H}^{(1)}_n(\alpha^{[1]S}),\\
\mathcal{D}_n(2,4) &= -\mathrm{i}nJ_n(\alpha^{[2]P}),\\
\mathcal{D}_n(2,5) &= \alpha^{[2]S}\dot{J}_n(\alpha^{[2]S}),\\
\mathcal{D}_n(3,1) &= (1-\mu^{[1]}_P)\alpha^{[1]P}\dot{H}^{(1)}_n(\alpha^{[1]P}),\\
\mathcal{D}_n(3,2) &= (1-\mu^{[1]}_A)\alpha^{[1]A}\dot{H}^{(1)}_n(\alpha^{[1]A}),\\
\mathcal{D}_n(3,3) &= \mathrm{i}n(1-\mu^{[1]}_S)\dot{H}^{(1)}_n(\alpha^{[1]S}),\\
\mathcal{D}_n(3,4) &= 0,\\
\mathcal{D}_n(3,5) &= 0,\\
\mathcal{D}_n(4,1) &= (a_P+b_P)(\alpha^{[1]P})^2H^{(1)}_n(\alpha^{[1]P}) + 2N(\alpha^{[1]P})^2\ddot{H}_n(1)(\alpha^{[1]P}),\\
\mathcal{D}_n(4,2) &= (a_A+b_A)(\alpha^{[1]A})^2H^{(1)}_n(\alpha^{[1]A}) + 2N(\alpha^{[1]A})^2\ddot{H}_n(1)(\alpha^{[1]A}),\\
\mathcal{D}_n(4,3) &= 2\mathrm{i}nN(-H^{(1)}_n(\alpha^{[1]S}) + \alpha^{[1]S}\dot{H}^{(1)}_n(\alpha^{[1]S})),\\
\mathcal{D}_n(4,4) &= (\alpha^{[2]P})^2(\lambda^{[2]}J_n(\alpha^{[2]P}) - 2\mu^{[2]}\ddot{J}_n(\alpha^{[2]P})),\\
\mathcal{D}_n(4,5) &= -2\mathrm{i}n\mu^{[2]}(-J_n(\alpha^{[2]S}) + \alpha^{[2]S}\dot{J}_n(\alpha^{[2]S})),\\
\mathcal{D}_n(5,1) &= 2\mathrm{i}nN(-H^{(1)}_n(\alpha^{[1]P}) + \alpha^{[1]P}\dot{H}^{(1)}_n(\alpha^{[1]P})),\\
\mathcal{D}_n(5,2) &= 2\mathrm{i}nN(-H^{(1)}_n(\alpha^{[1]A}) + \alpha^{[1]A}\dot{H}^{(1)}_n(\alpha^{[1]A})),\\
\mathcal{D}_n(5,3) &= N(-n^2H^{(1)}_n(\alpha^{[1]S}) + \alpha^{[1]S}\dot{H}^{(1)}_n(\alpha^{[1]S}) - (\alpha^{[1]S})^2\ddot{H}_n(1)(\alpha^{[1]S})),\\
\mathcal{D}_n(5,4) &= -2\mathrm{i}n\mu^{[2]}(-J_n(\alpha^{[2]P}) + \alpha^{[2]P}\dot{J}_n(\alpha^{[2]P})),\\
\mathcal{D}_n(5,5) &= -\mu^{[2]}(-n^2J_n(\alpha^{[2]S}) + \alpha^{[2]S}\dot{J}_n(\alpha^{[2]S}) - (\alpha^{[2]S})^2\ddot{J}_n(\alpha^{[2]S})),
\end{aligned}
\tag{B2}
$$

where $\alpha^{[i]X} = k^{[i]X}a$ for $X = P,A,S$ and $i = 1,2$; $a_X = 2N - P - Q\mu_X$ and $b_X = -(Q + R\mu_X)$ for $X = P,A$; $\dot{J}_n$, $\ddot{J}_n$, $\dot{H}_n^{(1)}$, and $\ddot{H}_n(1)$ denote the first and second derivatives of both the Bessel and Hankel functions, respectively, with regard to r. The source terms s_n^X are also given by

$$
\begin{aligned}
s_n^X(1) &= -\alpha^{[1]X}\dot{J}_n(\alpha^{[1]X}),\\
s_n^X(2) &= -\mathrm{i}nJ_n(\alpha^{[1]X}),\\
s_n^X(3) &= -(1-\mu_X^{[1]})\alpha^{[1]X}\dot{J}_n(\alpha^{[1]X}),\\
s_n^X(4) &= -(a_X+b_X)(\alpha^{[1]X})^2J_n(\alpha^{[1]X}) - 2N(\alpha^{[1]X})^2J_n(\alpha^{[1]X}),\\
s_n^X(5) &= -2N\mathrm{i}n(-J_n(\alpha^{[1]X}) + \alpha^{[1]X}\dot{J}_n(\alpha^{[1]X})),
\end{aligned}
\tag{B3}
$$

for $X = P$, A and

$$
\begin{aligned}
s_n^S(1) &= -\mathrm{i}nJ_n(\alpha^{[1]S}),\\
s_n^S(2) &= \alpha^{[1]S}\dot{J}_n(\alpha^{[1]S}),\\
s_n^S(3) &= -\mathrm{i}n(1-\mu_S^{[1]})J_n(\alpha^{[1]S}),\\
s_n^S(4) &= -2N\mathrm{i}n(-J_n(\alpha^{[1]S}) + \alpha^{[1]S}\dot{J}_n(\alpha^{[1]S})),\\
s_n^S(5) &= -N(-n^2J_n(\alpha^{[1]S}) + \alpha^{[1]S}J_n(\alpha^{[1]S}) - (\alpha^{[1]S})^2\ddot{J}_n(\alpha^{[1]S})).
\end{aligned}
\tag{B4}
$$

In the case of a shell elastic inclusion filled with air, as studied in the second configuration introduced Sec. III B, the previously evaluated boundary conditions at $r = a$ are supplemented by those at the shell/air interface at $r = b = a - h$,

$$
u_r^{[0]} = u_r^{[2]}, \quad -p^{[0]} = \sigma_{rr}^{[2]}, \quad 0 = \sigma_{r\theta}^{[2]}. \tag{B5}
$$

The size of the scattering problem is therefore extended to account for the waves inside the shell inclusion and the wave transmitted to the inner air medium, leading to the following vector of unknowns

$$
\boldsymbol{t}_n^X = [\,T_n^{XP} \quad T_n^{XA} \quad T_n^{XS} \quad E_n^{XP} \quad E_n^{XS} \quad F_n^{XP} \quad F_n^{XS} \quad T_n^X\,]^T. \tag{B6}
$$

The associated coefficients inside the extended scattering matrix $\mathcal{D}_n \in \mathbb{C}^{8,8}$ are given by

$$
\begin{aligned}
\mathcal{D}_n(1,6) &= -\alpha^{[2]P}\dot{H}_n^{(1)}(\alpha^{[2]P}),\\
\mathcal{D}_n(1,7) &= -\mathrm{i}nH_n^{(1)}(\alpha^{[2]S}),\\
\mathcal{D}_n(1,8) &= 0,\\
\mathcal{D}_n(2,6) &= -\mathrm{i}nH_n^{(1)}(\alpha^{[2]P}),\\
\mathcal{D}_n(2,7) &= \alpha^{[2]S}\dot{H}_n^{(1)}(\alpha^{[2]S}),\\
\mathcal{D}_n(2,8) &= 0,\\
\mathcal{D}_n(3,6:8) &= 0,\\
\mathcal{D}_n(4,6) &= (\alpha^{[2]P})^2(\lambda^{[2]}H_n^{(1)}(\alpha[2]P) - 2\mu^{[2]}\ddot{H}_n(1)(\alpha[2]P)),\\
\mathcal{D}_n(4,7) &= -2\mathrm{i}n\mu^{[2]}(-H_n^{(1)}(\alpha^{[2]S}) + \alpha^{[2]S}\dot{H}_n^{(1)}(\alpha^{[2]S})),\\
\mathcal{D}_n(4,8) &= 0,\\
\mathcal{D}_n(5,6) &= -2\mathrm{i}n\mu^{[2]}(-H_n^{(1)}(\alpha^{[2]P}) + \alpha^{[2]P}\dot{H}_n^{(1)}(\alpha^{[2]P})),\\
\mathcal{D}_n(5,7) &= -\mu^{[2]}(-n^2H_n^{(1)}(\alpha^{[2]S}) + \alpha^{[2]S}\dot{H}_n^{(1)}(\alpha^{[2]S}) - (\alpha^{[2]S})^2\ddot{H}_n(1)(\alpha^{[2]S})),\\
\mathcal{D}_n(5,8) &= 0,\\
\mathcal{D}_n(6,1:3) &= 0,\\
\mathcal{D}_n(6,4) &= -\beta^{[2]P}\dot{J}_n(\beta^{[2]P}),\\
\mathcal{D}_n(6,5) &= -\mathrm{i}nJ_n(\beta^{[2]P}),\\
\mathcal{D}_n(6,6) &= -\beta^{[2]P}\dot{H}_n^{(1)}(\beta^{[2]P}),\\
\mathcal{D}_n(6,7) &= -\mathrm{i}nH_n^{(1)}(\beta^{[2]P}),\\
\mathcal{D}_n(6,8) &= \beta^{[0]}\dot{J}_n(\beta^{[0]})/(\rho^{[0]}\omega^2),
\end{aligned}
\tag{B7}
$$

$$
\begin{aligned}
&\mathcal{D}_n(7,1:3)=0,\\
&\mathcal{D}_n(7,4)=-(\beta^{[2]P})^2(\lambda^{[2]}J_n(\beta[2]P)-2\mu^{[2]}\ddot{J}_n(\beta[2]P)),\\
&\mathcal{D}_n(7,5)=2in\mu^{[2]}(-J_n(\beta^{[2]S})+\beta^{[2]S}\dot{J}_n(\beta^{[2]S})),\\
&\mathcal{D}_n(7,6)=-(\beta^{[2]P})^2(\lambda^{[2]}H_n^{(1)}(\beta[2]P)-2\mu^{[2]}\ddot{H}_n(1)(\beta[2]P)),\\
&\mathcal{D}_n(7,7)=2in\mu^{[2]}(-H_n^{(1)}(\beta^{[2]S})+\beta^{[2]S}\dot{H}_n^{(1)}(\beta^{[2]S})),\\
&\mathcal{D}_n(7,8)=b^2J_n(\beta^{[0]}),\\
&\mathcal{D}_n(8,1:3)=0,\\
&\mathcal{D}_n(8,4)=-2in\mu^{[2]}(\beta^{[2]P}\dot{J}_n(\beta^{[2]P})-J_n(\beta^{[2]P})),\\
&\mathcal{D}_n(8,5)=-\mu^{[2]}(-(\beta^{[2]S})^2\ddot{J}_n(\beta^{[2]S})+\beta^{[2]S}\dot{J}_n(\beta^{[2]S})-n^2J_n(\beta^{[2]S})),\\
&\mathcal{D}_n(8,6)=-2in\mu^{[2]}(\beta^{[2]P}\dot{H}_n^{(1)}(\beta^{[2]P})-H_n^{(1)}(\beta^{[2]P})),\\
&\mathcal{D}_n(8,7)=-\mu^{[2]}(-(\beta^{[2]S})^2\ddot{H}_n(1)(\beta^{[2]S})+\beta^{[2]S}\dot{H}_n^{(1)}(\beta^{[2]S})-n^2H_n^{(1)}(\beta^{[2]S})),\\
&\mathcal{D}_n(8,8)=0,
\end{aligned}
\tag{B8}
$$

where $\beta^{[i]X}=k^{[i]X}b$ for $X=P$, A, S and $i=1$, 2. The associated source terms are identical to the previous ones with additional components equal to zero.

APPENDIX C: DETAILS OF THE SEMI-ANALYTICAL FORMULATION

To ease the understanding of the theoretical developments exposed in Sec. II D, the following coefficients have been defined

$$
\begin{aligned}
Q_{mnq}^{XY}=\mathrm{i}^n[&\cos(n\xi_q^Y-k_{2q}^{[1]Y}x_2^{(0)})({}^{(i)}\mathcal{F}_{qm}^X+{}^{(j)}\mathcal{F}_{qm}^X)\\
&+\mathrm{i}\sin(n\xi_q^Y-k_{2q}^{[1]Y}x_2^{(0)})\\
&\times({}^{(i)}\mathcal{F}_{qm}^X-{}^{(j)}\mathcal{F}_{qm}^X)]e^{\mathrm{i}k_{1q}x_1^{(0)}},
\end{aligned}
\tag{C1}
$$

and concerning the initial incident source terms

$$
\begin{aligned}
S_{nq}^Y=\mathrm{i}^n[&\cos(n\xi_q^Y-k_{2q}^{[1]Y}x_2^{(0)})({}^{(i)}\mathcal{F}_q^{\mathrm{inc}}+{}^{(j)}\mathcal{F}_q^{\mathrm{inc}})\\
&+\mathrm{i}\sin(n\xi_q^Y-k_{2q}^{[1]Y}x_2^{(0)})\\
&\times({}^{(i)}\mathcal{F}_q^{\mathrm{inc}}-{}^{(j)}\mathcal{F}_q^{\mathrm{inc}})]e^{\mathrm{i}k_{1q}x_1^{(0)}}\delta_q,
\end{aligned}
\tag{C2}
$$

where "$\cdot^{(i)}$." and "$\cdot^{(j)}$." represent the line numbers inside $\boldsymbol{f}_q$ corresponding to the concerned Y-type wave.

APPENDIX D: NUMERICAL RECIPES

Considering the complexity of the derived linear systems resulting from both Biot's formulation and the transition operators, partial numerical solutions are performed. Hence, the various infinite sums must be truncated according to the following criteria:

- for the modal representation of the field scattered by a single inclusion

$$
\begin{aligned}
N=\mathrm{int}(&\mathrm{Re}\{4.05\min([k^{[1]P}\,k^{[1]A}\,k^{[1]S}]a)^{1/3}\\
&+\min([k^{[1]P}\,k^{[1]A}\,k^{[1]S}]a)\})+10,
\end{aligned}
\tag{D1}
$$

- for the sum over the array of inclusions, which depends on the considered frequency and the periodicity of the array

$$
\begin{aligned}
P=\mathrm{int}\Bigg[\frac{d}{2\pi}\Big(&3\,\mathrm{Re}\{\max([k^{[1]P}\,k^{[1]A}\,k^{[1]S}])\}\\
&-\mathrm{Re}\{k_1^{\mathrm{inc}}\}\Big)\Bigg]+5,
\end{aligned}
\tag{D2}
$$

- for the lattice sum, which can be seen as a dissipative Schlömilch series, the following stopping criterion is used:

$$
\begin{aligned}
&\left|\mathrm{Re}\left\{\frac{\sigma_{mn}^{(L+1)}-\sigma_{mn}^{(L)}}{\sigma_{mn}^{(L)}}\right\}\right|\le 10^{-6}\quad\text{and}\\
&\left|\mathrm{Im}\left\{\frac{\sigma_{mn}^{(L+1)}-\sigma_{mn}^{(L)}}{\sigma_{mn}^{(L)}}\right\}\right|\le 10^{-6},
\end{aligned}
\tag{D3}
$$

where superscripts "$\cdot^{(L)}$" and "$\cdot^{(L+1)}$" indicate the truncation order of the series. It must be noticed that the losses accounted for through the complex wave numbers in Eq. (25) highly contribute to a quick convergence of these series.

[1]O. Tanneau, J.-B. Casimir, and P. Lamary, "Optimization of multilayered panels with poroelastic components for an acoustical transmission objective," J. Acoust. Soc. Am. **120**, 1227–1238 (2006).
[2]X. Olny and C. Boutin, "Acoustic wave propagation in double porosity media," J. Acoust. Soc. Am. **114**, 73–89 (2003).
[3]C. Boutin, P. Royer, and J. L. Auriault, "Acoustic absorption of porous surfacing with dual porosity," Int. J. Solids Struct. **35**(34–35), 4709–4737 (1998).
[4]F. C. Sgard, F. Castel, and N. Atalla, "Use of a hybrid adaptative finite element/modal approach to assess the sound absorption of porous materials with meso-heterogeneities," Appl. Acoust. **72**, 157–168 (2011).
[5]F. C. Sgard, X. Olny, N. Atalla, and F. Castel, "On the use of perforations to improve the sound absorption of porous materials," Appl. Acoust. **66**, 625–651 (2005).
[6]J. S. Lee, Y. Y. Kim, and Y. J. Kang, "Two-dimensional poroelastic acoustical foam shape design for absorption coefficient maximization by topology optimization method," J. Acoust. Soc. Am. **123**, 2094–2106 (2008).

[7]A. Gourdon and M. Seppi, "On the use of porous inclusions to improve the acoustical response of porous materials: Analytical model and experimental verification," Appl. Acoust. **71**, 283–298 (2010).
[8]L. De Ryck, J.-P. Groby, P. Leclaire, W. Lauriks, A. Wirgin, Z. E. A. Fellah, and C. Depollier, "Acoustic wave propagation in a macroscopically inhomogeneous porous medium saturated by a fluid," Appl. Phys. Lett. **90**, 181901 (2007).
[9]M. A. Biot, "Generalized theory of acoustic propagation in porous dissipative media," J. Acoust. Soc. Am. **34**(5), 1254–1264 (1962).
[10]G. Gautier, L. Kelders, J.-P. Groby, O. Dazel, L. De Ryck, and P. Leclaire, "Propagation of acoustic waves in a one-dimensional macroscopically inhomogeneous poroelastic material," J. Acoust. Soc. Am. **130**, 1390–1398 (2011).
[11]C. J. Naify and S. Nutt, "Multifunctional acoustic metamaterial composites," J. Acoust. Soc. Am. **130**(4), 2326 (2011).
[12]A. N. Norris and M. R. Haberman, "Introduction to the Special Issue on Acoustic Metamaterials," J. Acoust. Soc. Am. **132**(4), 2783 (2012).
[13]J. Sanchez-Dehesa and D. Torrent, "Acoustic metamaterials based on phononic crystals," J. Acoust. Soc. Am. **128**, 2427 (2010).
[14]O. Umnova, K. Attenborough, and C. Linton, "Effects of porous covering on sound attenuation by periodic array of cylinders," J. Acoust. Soc. Am. **119**(1), 278–284 (2006).
[15]Z. Yang, H. M. Dai, N. H. Chan, G. C. Ma, and P. Sheng, "Acoustic metamaterial panels for sound attenuation in the 50–1000 Hz regime," Appl. Phys. Lett. **96**(4), 041906 (2010).
[16]V. Tournat, V. Pagneux, D. Lafarge, and L. Jaouen, "Multiple scattering of acoustic waves and porous absorbing media," Phys. Rev. E **70**, 026609 (2004).
[17]R. W. Wood, "A suspected case of the electrical resonance of minute metal particles for light-waves. A new type of absorption," Proc. Physiol. Soc. (London, U. K.) **18**, 166–182 (1902).
[18]A. Wirgin and T. Lopez-Rios, "Can surface-enhanced Raman scattering be caused by waveguide resonances?," Opt. Commun. **48**, 416–420 (1984).
[19]J.-P. Groby, A. Wirgin, E. Ogam, L. De Ryck, W. Lauriks, and C. Depollier, "Acoustic response of a soniclike crystal within a rigid frame porous plate," J. Acoust. Soc. Am. **123**, 3039 (2008).
[20]J.-P. Groby, O. Dazel, A. Duclos, L. Boeckx, and L. Kelders, "Enhancing the absorption coefficient of a backed rigid frame porous layer by embedding circular periodic inclusions," J. Acoust. Soc. Am. **130**, 3771–3780 (2011).
[21]C. Lagarrigue, J.-P. Groby, V. Tournat, O. Dazel, and O. Umnova, "Absorption of sound by porous layers with embedded periodic arrays of resonant inclusions," J. Acoust. Soc. Am. **134**(6), 4670–4680 (2013).
[22]J.-P. Groby, C. Lagarrigue, B. Brouard, O. Dazel, V. Tournat, and B. Nennig, "Using simple shape three-dimensional rigid inclusions to enhance porous layer absorption," J. Acoust. Soc. Am. **136**(3), 1139–1148 (2014).
[23]J.-P. Groby, C. Lagarrigue, B. Brouard, O. Dazel, V. Tournat, and B. Nennig, "Enhancing the absorption properties of acoustic porous plates by periodically embedding Helmholtz resonators," J. Acoust. Soc. Am. **137**(1), 273–280 (2015).
[24]M. A. Biot, "Theory of propagation of elastic waves in a fluid-saturated porous solid. I. Low-frequency range," J. Acoust. Soc. Am. **28**(2), 168–178 (1956).
[25]Y. Champoux and J. F. Allard, "Dynamic tortuosity and bulk modulus in air-saturated porous media," J. Appl. Phys. **70**(4), 1975–1979 (1991).
[26]J. F. Allard and N. Atalla, *Propagation of Sound in Porous Media*, 2nd ed. (Wiley, Chichester, UK, 2009), pp. 111–123.
[27]V. K. Varadan, "Multiple scattering of acoustic, electromagnetic and elastic waves," in *Acoustic, Electromagnetic and Elastic Wave Scattering—Focus on the T-Matrix Approach*, edited by V. K. Varadan and V. V. Varadan (Pergamon, New York, 1980), pp. 103–134.
[28]Y. Liu, R. S. Wu, and C. F. Fing, "Scattering of elastic waves by an elastic or vicoelastic cylinder," Geophys. J. Int. **142**, 439–460 (2000).
[29]S. M. Hasheminejad and R. Avazmohammadi, "Acoustic diffraction by a pair of poroelastic cylinders," J. Appl. Math. Mech. **86**(8), 589–605 (2006).
[30]C. Zimmerman and M. Stern, "Scattering of plane compressional waves by spherical inclusions in a poroelastic medium," J. Acoust. Soc. Am. **94**(1), 527–536 (1993).
[31]F. Záviška, "Über die beugung elektromagnetischer wellen an parallelen, unendlich langen kreiszylindern" ("On the diffraction of electromagnetic waves by parallel, infinitely long cylinders"), Ann. Phys. **345**(5), 1023–1056 (1913).
[32]V. Twersky, "Multiple scattering of radiation by an arbitrary configuration of parallel cylinders," J. Acoust. Soc. Am. **24**, 42–46 (1952).
[33]S. Robert, "Propagation d'ondes cohérentes et résonances dans des milieux élastiques présentant des inclusions cylindriques périodiquement ou aléatoirement distribuées" ("Propagation of coherent waves and resonances in elastic media presenting cylindrical inclusions periodically or randomly distributed"), Ph.D. thesis, Université du Havre, 2004.
[34]F. Luppé, J.-M. Conoir, and S. Robert, "Coherent waves in a multiply scattering poro-elastic medium obeying Biot's theory," Waves Random Complex Media **18**, 241–254 (2008).
[35]J.-P. Groby, A. Wirgin, and E. Ogam, "Acoustic response of a periodic distribution of macroscopic inclusions within a rigid frame porous plate," Waves Random Complex Media **18**(3), 409–433 (2008).
[36]J.-P. Groby, A. Wirgin, L. De Ryck, W. Lauriks, R. P. Gilbert, and Y. S. Xu, "Acoustic response of a rigid-frame porous medium plate with a periodic set of inclusions," J. Acoust. Soc. Am. **126**, 685–693 (2009).
[37]T. Cox and P. D'Antonio, *Acoustic Absorbers and Diffusers: Theory, Design and Application* (Taylor and Francis, Abingdon, Oxon, UK, 2009), pp. 196–229.
[38]G. Ma, M. Yang, S. Xiao, Z. Yang, and P. Sheng, "Acoustic metasurface with hybrid resonances," Nat. Mater. **13**, 873–878 (2014).
[39]V. Romero-Garcia, G. Theocharis, O. Richoux, A. Merkel, V. Tournat, and V. Pagneux, "Perfect and broadband acoustic absorption by critically coupled sub-wavelength resonators," Sci. Rep. **6**, 19519 (2016).
[40]T. G. Zieliński, "Numerical investigation of active porous composites with enhanced acoustic absorption," J. Sound Vib. **330**, 5292–5308 (2011).
[41]O. Dazel, F. Sgard, F.-X. Bécot, and N. Atalla, "Expressions of dissipated powers and stored energies in poroelastic media modeled by $\{u,U\}$ and $\{u,P\}$ formulations," J. Acoust. Soc. Am. **123**, 2054–2063 (2008).
[42]J. Mei, G. Ma, M. Yang, Z. Yang, W. Wen, and P. Sheng, "Dark acoustic metamaterials as super absorbers for low-frequency sound," Nat. Commun. **3**, 756 (2012).
[43]A. Norris and G. Wickham, "Elastic Helmholtz resonators," J. Acoust. Soc. Am. **93**, 617–630 (1993).